Ultrasound Triggered ZnO-Based Devices for Tunable and Multifaceted Biomedical Applications

ADVANCED MATERIALS INTERFACES
www.advmatinterfaces.de

Ultrasound Triggered ZnO-Based Devices for Tunable and Multifaceted Biomedical Applications

*Marco Carofiglio, Marco Laurenti, Giada Graziana Genchi, Gianni Ciofani, Marta Grochowicz, and Valentina Cauda**

Smart materials able to respond to an external stimulus or an environmental condition represent milestone developments in modern medicine. Among them, zinc oxide (ZnO) is a highly intriguing inorganic material with versatile morphologies/shapes and multifunctional properties like piezoelectricity, enhanced reactive oxygen species (ROS) generation, and antimicrobial ones. Here, the fabrication of smart ZnO-based films is shown that can remotely be activated by ultrasound (US). US exposure induces electrical potentials on the fabricated devices that can be exploited to stimulate electrically responsive cells or promote ROS generation for cancer treatment. ZnO microparticles with surface nanostructuring are thus synthesized and processed in the form of a paste to deposit thin films on flexible polymeric supports. ZnO paste formulation and the fabrication procedure of the final device are optimized in terms of uniformity, hydrophilicity, and purity. Graphene oxide and poly(2-hydroxyethyl methacrylate) are also layered onto the ZnO films in order to provide the devices with additional functionalities. ROS generation and electro-mechanical performances upon US stimulation are evaluated for all of the developed devices. Finally, biocompatibility studies are conducted with osteoblast-like cell cultures for possible applications in the contexts of bone tissue engineering/therapy.

1. Introduction

The research on nanostructured materials and technology in biomedicine is relatively recent but its application has already shown how big their potentialities are. However, biomedicine is a tremendously vast subject that pervades its roots in several fields, like tissue engineering, neurological disorders, or oncology. Clearly, each application has specific requirements that need to be fulfilled when a new device has to be designed.

Micro and nanotechnologies play an important role in this sense because they allow to act directly on the cellular and intracellular level,[1] introducing novel possibilities in terms of therapy and early diagnosis. Moreover, nanoengineering is paving the way to a brand new class of devices which are able to react to external stimuli and induce specific reactions to the target biological entity,[2] acting either as therapeutic or diagnostic agent.

An example of external stimulus is represented by the electric potential which can be induced by the physical deformation of a piezoelectric material or, more in general, an electro-mechanically active device. As a matter of fact, piezoelectricity could be effectively used to convert a mechanical stimulation into an electrical one. The mechanical stimulus can come endogenously, that is, from the interior of the body, like the movement of muscles, respiration, or heartbeat.[3] Alternatively, the mechanical stimulation can be exogenous, that is, obtained from a stimulation exterior to the body, like the periodical pressure waves provided by an ultrasound (US) irradiation.[4] Indeed, several works report how the electromechanical conversion effect can be used to induce growth or differentiation to electrical stimulation sensitive cells like neurons,[5,6] muscles,[7] or bone tissues.[8] The role of the electric potential is to induce a disequilibrium in cell ions homeostasis, leading to different cellular pathways which range from cell differentiation[9,10] to antitumoral drug cell sensitization[11] according to the provided stimulation.

A lot of research has also focused on the generation on demand of reactive oxygen species (ROS) in order to induce either cancer cell death or improve vascularization in healthy tissues. Several physical stimuli can be exploited with the purpose of generating ROS in biomedicine[12] like light[13,14] or USs. Considering only ultrasonic stimulations, sonodynamic therapy is based on the inertial cavitation induced by ultrasonic acoustic pressure waves on gas micro-bubbles trapped in the aqueous media in which cells are immersed. The implosion of these bubbles caused by the periodical pressure wave provides the

M. Carofiglio, M. Laurenti, V. Cauda
Department of Applied Science and Technology
Politecnico di Torino
Corso Duca degli Abruzzi 24, Turin 10129, Italy
E-mail: valentina.cauda@polito.it
G. G. Genchi, G. Ciofani
Istituto Italiano di Tecnologia
Smart Bio-Interfaces
Viale Rinaldo Piaggio 34, Pontedera (Pisa) 56025, Italy
M. Grochowicz
Department of Polymer Chemistry
Maria Curie Sklodowska University
Gliniana 33, Lublin 20-614, Poland
The ORCID identification number(s) for the author(s) of this article can be found under https://doi.org/10.1002/admi.202101021.

DOI: 10.1002/admi.202101021

release of a high amount of energy in water which induces radicals formation.[15]

Indeed, the possibilities in terms of physical stimulations are many as well as challenging to be optimized. For this reason, versatile materials assumed a tremendous relevance in medical sciences thanks to their possibility to be engineered in several ways to reach this goal.

The development of new generation devices based on zinc oxide (ZnO) micro and nanostructures, for example, is gaining an important place among various biomedical fields like tissue engineering,[16] fight against cancer,[13,17,18] sensors,[19–23] and controlled drug release[24] thanks to ZnO intrinsic antimicrobial,[25,26] photocatalytic,[27,28] piezoelectric[29,30] properties and its bioimaging potentialities.[31]

Among the various features, ZnO presents extreme possibility to be customized in terms of size and morphology. Both these tuning parameters allow to obtain either nanoparticles, able to penetrate tissues and act as an intracellular sensitizing agent for photo-[13,32] or sono-dynamic[15,33,34] therapies, or porous structures that can be exploited for a controlled drug release,[24,35] or even micro-sized materials with high electromechanical or photoconductive features exploitable as thin films or layers.

The aim of this works is to develop a new and extremely versatile device that is able to exploit all the interesting properties of ZnO. In particular, zinc oxide microparticles with nanostructured surface were selected to fabricate smart supports able to generate an electrical potential under the application of an external mechanical stimulus, that is, US stimulation. In view of this property, a remote US stimulation is provided to the ZnO support to be used to electrically stimulate cells. Second, the presence of a highly nanostructured ZnO surface exposed to US in water-based media is also reported to induce an enhanced acoustic cavitation effect and thus the generation of ROS. In order to exploit both effects, that is, electromechanical one and enhanced cavitation, the ZnO film was finely optimized in terms of film uniformity, by-products residuals, and hydrophilic behavior. In this way, a robust structure, which can stand further optimizations and additions of other nanomaterials or layer, was obtained. In particular, two types of hybrid inorganic/organic devices were fabricated and optimized starting from the pristine ZnO film. On the one hand, graphene oxide (GO) was deposited on top of the ZnO surface to tune the biocompatibility of the final device and increase the ROS generation potentialities under US stimulation. On the other hand, a biocompatible, conformable, and soft polymer, that is, poly(2-hydroxyethyl methacrylate) (pHEMA), was exploited to fabricate a hybrid device able to generate an electric potential by remote US stimulation.

The prepared samples were all characterized in terms of electric potential and ROS generation under US stimulation, to assess the performance of the devices. Finally, as a proof of concept, an osteosarcoma cell line (SaOS-2) was cultured on top of the devices to understand either the biocompatible properties or the cytotoxic capabilities of the fabricated devices.

These results, reported for the first time on a ZnO-based nanostructure materials coupled with GO or pHEMA, open the way to novel and promising multifunctional platforms for preparing devices with tunable biocompatibility and functionalities, showing efficient ROS generation and electro-mechanical performances upon US stimulation and useful for manifold biomedical applications.

2. Results and Discussions

The aim of this work is to fabricate ZnO films as remotely-activated smart material for biomedical applications. The device herein presented is obtained starting from highly porous, desert rose-like zinc oxide microparticles (DR-ZnO), which are then combined together in the form of thin film.

2.1. Powder Characterization

Before the fabrication of ZnO-based device, the ZnO powders synthesized with a sol-gel hydrothermal method were characterized in terms of morphology and crystal structure by means of Field Emission Scanning Electron Microscopy (FESEM) and X-ray diffraction (XRD) analyses.

As it can be seen from **Figure 1a**, the microparticles resulting from the synthesis are formed by the interpenetration of several lamellae having thickness of about 15 nm. The overall shape of the DR-ZnO microparticles is however spherical, with a diameter that ranges between 3 and 5 µm. Interestingly, despite the differences among microparticles regarding their diameter, the thickness of the various lamellae forming this peculiar shape does not vary significantly, indicating how

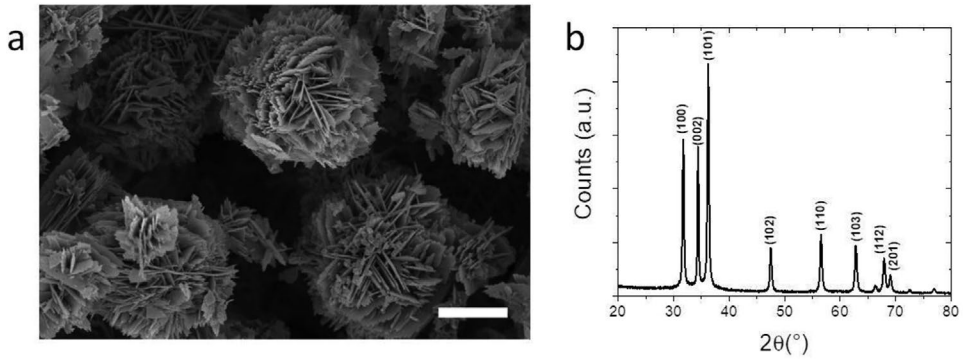

Figure 1. a) Representative FESEM image and b) XRD pattern of DR-ZnO microparticles. Scale bar is 1 µm.

the growth occurs in a precisely oriented manner, as also reported elsewhere.[36]

The XRD pattern reported in Figure 1b allows to recognize the single-phase wurtzitic structure of the resulting microparticles. Actually, all the peaks are attributed to the ones reported in JCPDS-ICDD (card n. 89-1397) for ZnO wurtzite structure. The intensity of the peaks also suggests a high level of crystallinity, while the average diameter of the crystallites could be evaluated by means of the Debye-Scherrer formula.[37]

The crystallite size was evaluated for the three main peaks finding values very close one to each other, that is, 25, 33, and 26 nm for the (100), (002), and (101) crystal planes, respectively. These values are even larger than the lamellae thickness found with FESEM measurements. Therefore, it is fair to assume that the lamellae are composed of a single crystallographic domain along their thickness, while they present several crystallographic grains in their other dimensions.

2.2. Optimization of ZnO Films Procedure

Once the powders have been synthesized, it is required to deposit them onto a substrate that is chemically inert and that presents the ability to sustain the thermal processes required to obtain the final device. This is the case of polyimide (PI), which is chemically and mechanically stable in a wide range of temperatures.[38] However, despite the good properties of this material, the deposition of DR-ZnO microparticles presents challenging criticalities due to the rapid precipitation of the microparticles in solvents like ethanol and water, and the poor wettability of the PI substrate which leads to easily detachable films.

An effective and rapid method to increase the wettability of PI and hence to improve both the stability and uniformity of the ZnO film is to perform an Argon plasma treatment onto the PI substrate prior to ZnO deposition. Different times of plasma treatments were considered and the surface wetting properties of the resulting PI samples analyzed in terms of optical contact angle (OCA). Before plasma treatment, the PI substrate presents an OCA of about 59° (Figure S1a, Supporting Information). Despite this value being already considered representative of a hydrophilic surface,[39] it is not enough to allow for a uniform coverage of the substrate by the ZnO particle dispersion (Figure S2a, Supporting Information). On the other hand, short plasma treatments are already very effective in reducing the OCA of PI up to values below 10° and no further reduction in the OCA values was observed by increasing the plasma time exposure (Figure S1b, Supporting Information). Therefore, a 2-min plasma treatment has been chosen as standard procedure for the optimal film fabrication.

The formulation of the ZnO paste used for preparing the final device accounts for the presence of acetic acid, which was exploited in a very small amount to enhance the dispersion of the ZnO microparticles inside the solution of water and ethanol as suggested by a visual estimation of the resulting DR-ZnO microparticles slurry. **Table 1** recalls all the pristine ZnO samples fabricated during the optimization procedure. The inclusion of acetic acid is required since the ZnO particles tend to aggregate and precipitate in water, while the introduction of acetic acid slightly modifies their surface chemistry, screening the interaction between ZnO and water. However, the presence of acetic acid leads to the formation of by-products that remain also after the first thermal treatment at 90 °C, exploited with the sole purpose of drying all the solvents.

Table 1. Samples analyzed during the optimization of the ZnO film fabrication.

Sample name	Acetic acid [% vol.]	Volume [mL]	ZnO powder [g]
PI-ZnO-A	0.8	2.325	1
PI-ZnO-B	0.8	2.325	0.5
PI-ZnO-C	0.4	2.315	0.5

In **Figure 2a**, a representative FESEM image of sample PI-ZnO-A prior to the 380 °C thermal treatment (whose preparation is described in Section 4.2) evidences some morphological differences related to the original microparticles. Indeed, it is possible to spot the presence of a foil-like morphology material that was not present in the ZnO powder. Attenuated total reflectance infrared spectroscopy (ATR-IR) and XRD analyses were exploited to establish the nature of by-products. In the ATR-IR spectrum of the film prior to 380 °C treatment (Figure 2b), it is possible to spot the presence of a broad band centered at 3600 cm^{-1}, which can be associated to the stretching vibrations of hydroxyl groups, and an intense peak rising close to 550 cm^{-1} that continues over the limit detectable by this ATR-IR set-up and which is related to the vibration of the Zn—O bond (typically reported to be at 440 cm^{-1}[40,41]). However, the most relevant information comes from the vibration peaks present at 1400 cm^{-1} and those between 1600 and 1500 cm^{-1} that can be ascribed to the deformation vibration of CH_3 bond[42] and to the asymmetric stretching mode of carboxylate group.[43] Indeed, both these peaks are found in compounds like zinc acetate ($(CH_3COO)_2Zn$) and basic zinc acetate ($Zn_4O(CH_3CO_2)_6$) which are supposed to be obtained by the slight dissolution of zinc oxide from acetic acid mixture during the film preparation. The XRD analysis reported in Figure 2c was exploited to discriminate between the two compounds. Indeed, apart from the peaks associated to the substrate and to the ZnO phase, in the 380 °C thermally un-treated sample XRD pattern, there is a peak centered at 6°. In another work exploiting a similar solvent composition for particles dispersion,[44] a similar peak is found and attributed to layered hydroxide zinc acetate (LHZA). To restore the original ZnO single phase by decomposition of LHZA, a thermal treatment at high temperature is exploited in this work.

With this aim, DR-ZnO films were thermally treated at 380 °C for 2 h and the samples analyzed again to validate this technique as effective in decomposing LHZA.

As it is possible to see in Figure 2a, all the foils that were formed during the deposition were eliminated during the process, leaving the microparticles composing the film completely exposed. Moreover, the LHZA removal was confirmed by the absence of its peak at 6° in the XRD pattern and the disappearance of the carbon-related peaks in the ATR-IR spectrum. As a final consideration, also the hydroxyl band is suppressed after this thermal treatment, probably because of its dehydration due to high temperatures.

Interestingly, the decomposition of the LHZA from the DR-ZnO film leads also to a different behavior of the surface in

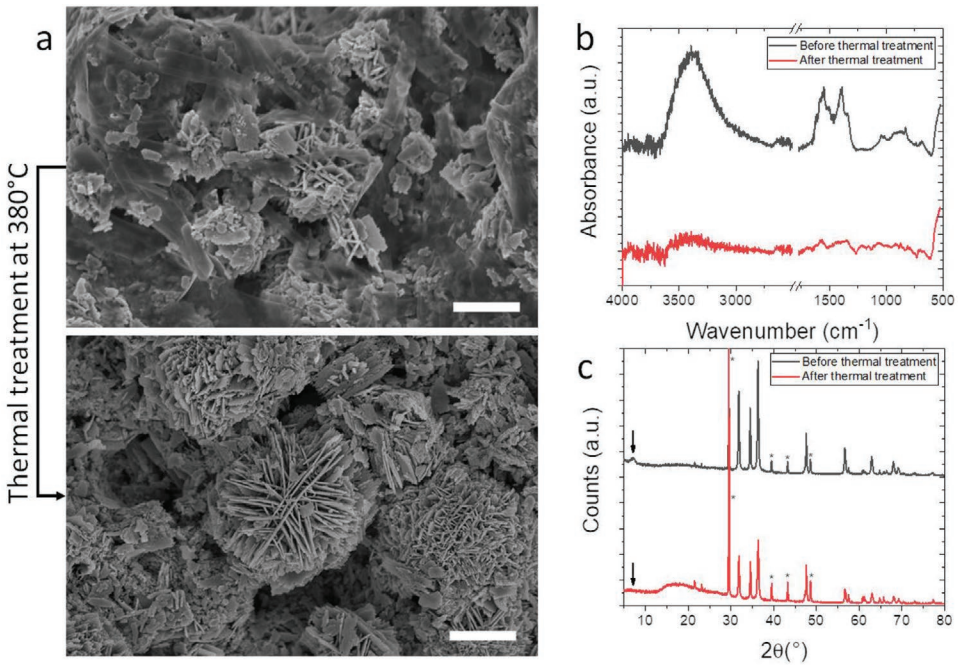

Figure 2. a) Representative FESEM images, b) ATR-IR spectroscopy, and c) XRD patterns (* refers to substrates peaks) of DR-ZnO film obtained with the PI-ZnO-A paste before and after 380 °C thermal treatment. Scale bar is 1 µm.

terms of hydrophilicity. Indeed, as it is possible to observe from **Figure 3a**, the ZnO layer presents an OCA of 70° when deposited and treated only at 90 °C for 30 min, while the OCA is lowered to 11° when the sample is treated at 380 °C for 2 h (Figure 3b). This result evidences how the thermal treatment is also required since a hydrophilic surface is typically needed for cell adhesion.[45]

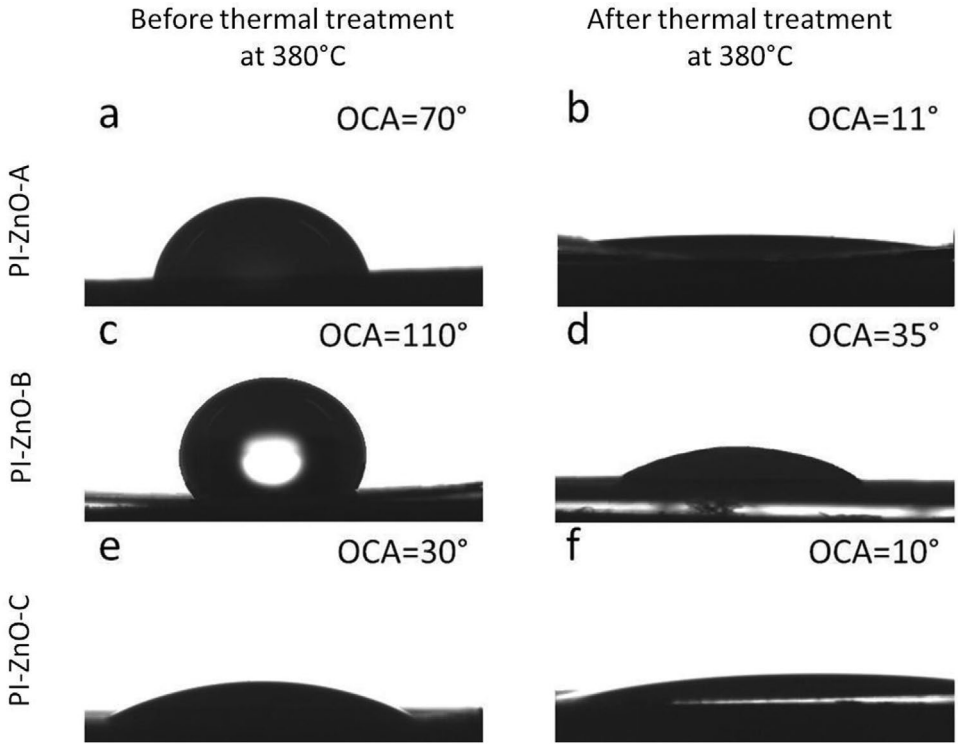

Figure 3. OCA of PI-ZnO films. PI-ZnO-A substrate a) before and b) after 380 °C thermal treatment, PI-ZnO-B substrate c) before and d) after 380 °C thermal treatment and PI-ZnO-C substrate e) before and f) after 380 °C thermal treatment.

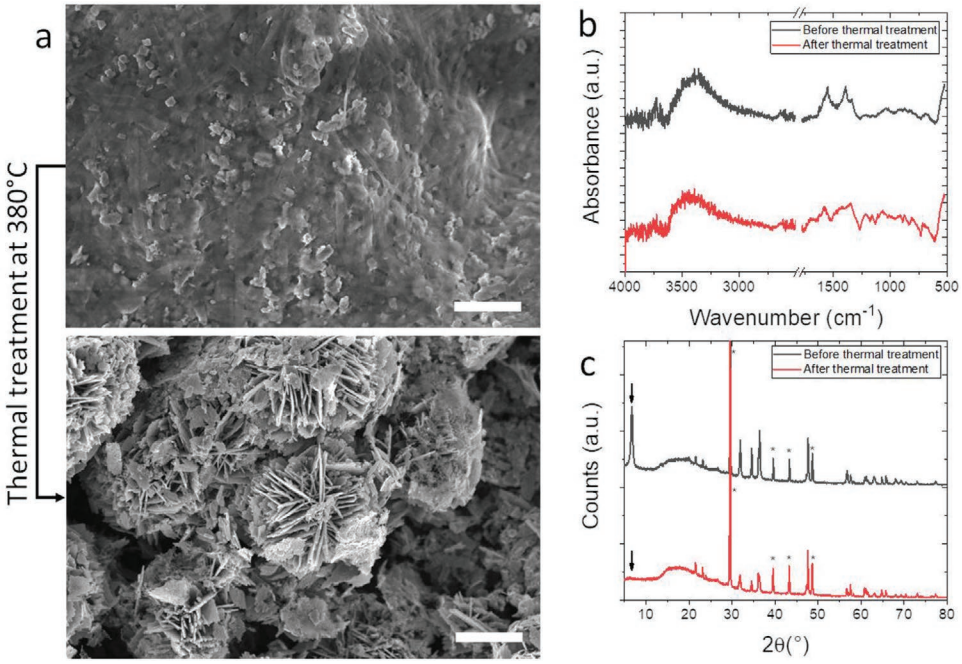

Figure 4. a) Representative FESEM images, b) ATR-IR spectroscopy, and c) XRD patterns (* refers to substrates peaks) of DR-ZnO film obtained with the PI-ZnO-B paste. Before and after treatment. Scale bar is 1 µm.

The samples obtained with the PI-ZnO-A paste formulation, whose results are summarized in Figure 2, presented some criticalities which made them not usable. As a matter of fact, despite the complete removal of the by-products during the deposition and the overall good uniformity, the thickness of the layer was too high and clusters of microparticles detached from the sample during handling and their introduction in a liquid medium (Figure S2b, Supporting Information). This was probably due to the poor adhesion of DR-ZnO microparticles to the PI substrate, which makes them unfeasible for biological applications where a good stability is required.

A reduction of the amount of ZnO per unit of volume of the solvent was then considered as an alternative to reduce the thickness of the film and therefore increase the stability of the device. In the system shown in **Figure 4** (PI-ZnO-B), the ratio of the solvent components was kept the same while the amount of ZnO dispersed was halved. The FESEM image on the film before thermal treatment (Figure 4a) clearly shows that the amount of LHZA formed during the fabrication of PI-ZnO-B is definitely higher than the amount produced in the case of PI-ZnO-A. Despite its complete removal after 380 °C thermal treatment, as also corroborated by ATR-IR and XRD analyses (Figure 4b,c, respectively), the resulting film does not present uniquely the DR-ZnO microparticles but also several foil-like residues on the film surface which could be attributed to the conversion of the LHZA foils into ZnO sheets partially deposited on the microparticles.

This phenomenon has a direct influence also on the OCA of the device, which presents a hydrophobic behavior before the thermal treatment at 380 °C (110°) and an OCA of 35° after the thermal treatment, that is, a higher OCA than the PI-ZnO-A sample (Figure 3c,d).

The reason for a higher production of LHZA may lay in the use of the same amount of acetic acid in a system in which the ZnO was halved in quantity. Therefore, the acetic acid is able to convert a large portion of ZnO into LHZA and difficulties in restoring the original morphology of the microparticles were found.

The solution to this problem is found by halving the amount of acetic acid, without any modification on the ethanol and water volumes. In this way, the amount of LHZA produced was sufficient to produce uniform films during deposition but do not induce major modifications on the morphology of the device. The films fabricated in this way (PI-ZnO-C) were considered optimal and thus exploited for further film characterizations and improvements to produce the hybrid devices.

FESEM, ATR-IR, and XRD analyses for sample PI-ZnO-C, before and after 380 °C thermal treatment, are reported in **Figure 5**. In particular, Figure 5a shows how the foils of LHZA on the device before the thermal treatment are clearly lower in number than the previous cases and that after the treatment there is no evidence of any microparticle morphology modification. Finally, ATR-IR and XRD patterns confirmed the complete removal of LHZA.

Moreover, this system revealed to be stable in both aqueous and cell culture media, without any detachment due to its introduction in liquid media and a lower OCA was found both prior and after 380 °C thermal treatment.

2.3. Organic Coating for the ZnO Films

To obtain hybrid inorganic/organic devices, a further modification of the PI-ZnO surface is proposed, including some organic materials like graphene oxide (GO) or poly(2-hydroxyethyl methacrylate) (pHEMA), in order

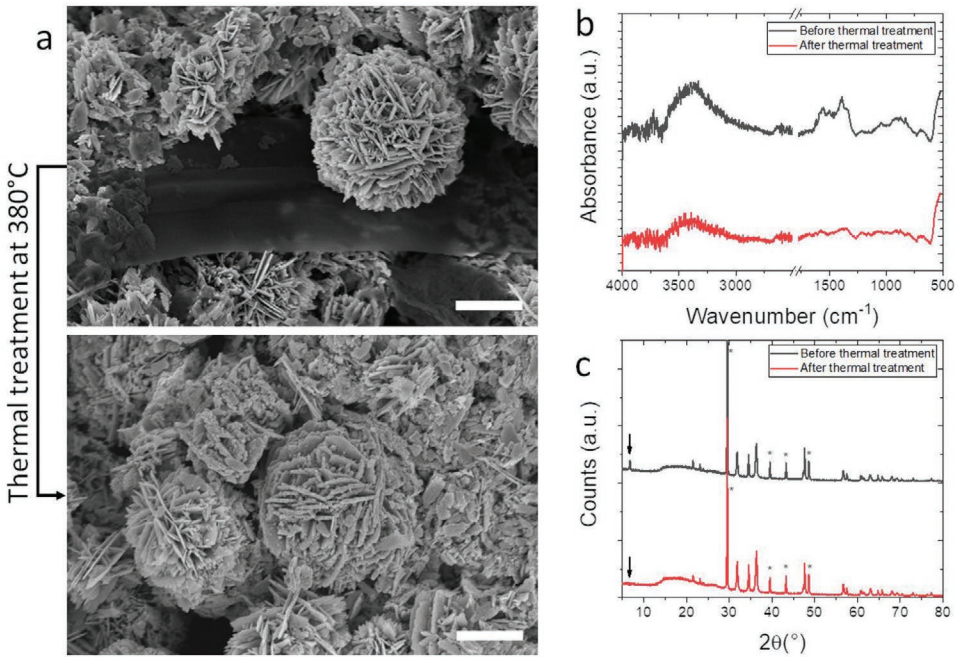

Figure 5. a) Representative FESEM images, b) ATR-IR spectroscopy, and c) XRD patterns (* refers to substrates peaks) of DR-ZnO film obtained with the PI-ZnO-C paste. Before and after treatment. Scale bar is 1 µm.

to add versatility to the system in terms of biomedical applications.

GO flakes have been already extensively used in several fields of technology thanks to the intriguing surface chemistry and lack of toxicity of GO.[46] It has also been already exploited with porous ZnO films with good results in terms of drug release control and bioactivity modulation.[35] Clearly, the possibility to include this material on the device can serve both as a method to tune the biocompatibility of the system and as a way to include new potentialities (i.e., drug-release control or ROS generation).

In this work, graphene oxide was deposited onto the ZnO film-based devices by drop-casting. The result was a continuous layer covering the whole ZnO sample surface, as is shown in the FESEM image reported in **Figure 6a**. The continuous layer suggests that this system can be effectively used to prevent an undesirable release of an eventually loaded drug in future. Interestingly, the main result of the inclusion of this GO layer is the introduction of new functional groups to the system, which could be exploited for further functionalization with either biomedical or electronic purposes.[47] For the specific case under analysis, the coating of the PI-ZnO with GO results in the inclusion of hydroxyl groups on the surface of the device, as indicated by the broad band in the 3600–3200 cm^{-1} region of the ATR-IR spectrum of the device.

Moreover, it is possible to observe the presence of peaks at ≈1600 and ≈1400 cm^{-1}, which could be related to the C=C stretching vibration[42] and to the deformation vibration of the OH groups in the C—OH functional group.[48]

As an alternative, pHEMA was also proposed as coating for the PI-ZnO-C samples. The selected hydrogel is typically recognized as a biocompatible material. In this work, pHEMA is conceived to act as a barrier layer preventing cell adhesion, to obtain a system that is able to perform antimicrobial activity (thanks to the well-recognized antibacterial properties of ZnO) but to avoid cell adhesion and biofilm formation at the same

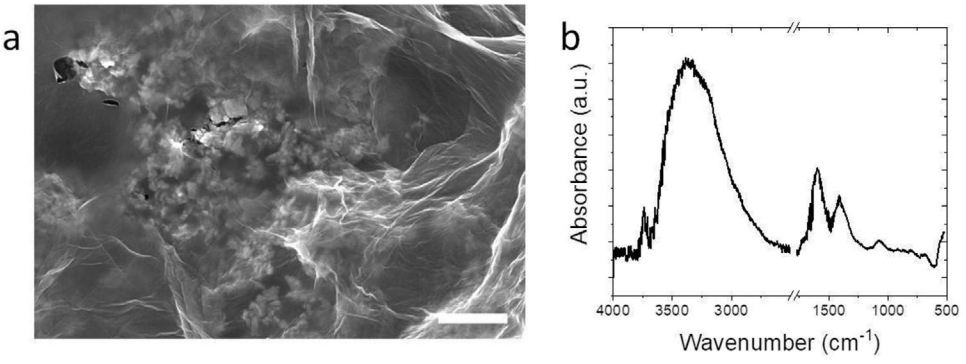

Figure 6. a) Representative FESEM images and b) ATR-IR spectroscopy of DR-ZnO film coated with graphene oxide by drop casting. Scale bar is 1 µm.

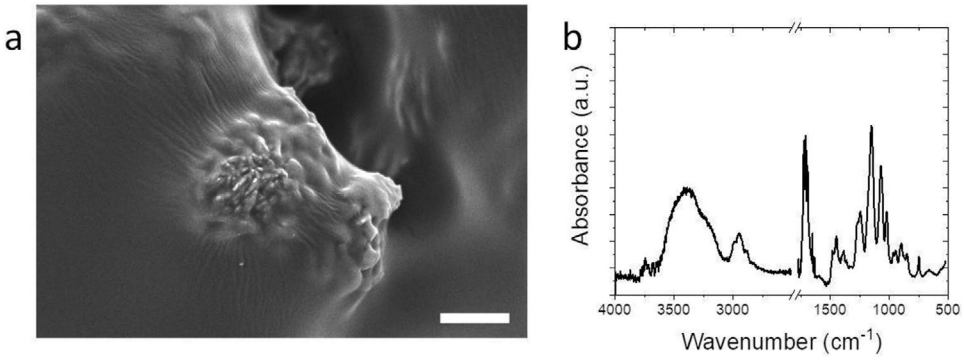

Figure 7. a) Representative FESEM images and b) ATR-IR spectroscopy of DR-ZnO film coated with pHEMA. Scale bar is 1 µm.

time. Both these aspects are particularly desirable for example in implants and catheters applications.[49,50] Drop casting was exploited also in this case to deposit pHEMA and the resulting coating was able to cover completely the ZnO microparticles. However, as it is shown in **Figure 7a**, by finely tuning the amount of deposited polymer, it is possible to have a coating which is not completely drowning ZnO, so that it can still contribute with antimicrobial properties.

In terms of chemical groups that are present on the surface, by means of the ATR-IR spectrum, it is possible to recognize as main peaks the hydroxyl group stretching vibration in the 3600–3100 cm^{-1} region, a peak in the region 2975–2860 cm^{-1} which could be related to aliphatic C—H stretching,[42] the carbonyl vibration[51] (1721 cm^{-1}) and the C—O stretching vibration[52] (1162 cm^{-1}).

2.4. Functional Films Characterization

The devices fabricated in this work were characterized in terms of electromechanical response to establish if these systems can be actually employed as active devices in biomedical treatments.

To do so, the maximum voltage generation between the top and the bottom surfaces of the device achieved when subjected to a US stimulation was measured for the three optimized devices (PI-ZnO-C, PI-ZnO-GO, and PI-ZnO-pHEMA), for simple PI (acting like a completely insulating system) and for PI-Cu sample (acting like a conductive system), both used as controls.

Figure 8a summarizes the results collected for the analyzed samples under different conditions of US powers and frequencies. As it can be seen, when the US power is kept fixed, the voltages of PI-ZnO-C, PI-ZnO-GO, and PI-Cu are one order of magnitude lower than the PI and PI-ZnO-pHEMA ones. The generation of an electric potential in these last devices can be first attributed to triboelectric phenomena given by the friction of the various layers composing the device. However, ZnO is also a piezoelectric material and its influence could also be considered.

Moreover, the different magnitudes of the electric potential found in the different systems can be attributed to the charge transport properties of the materials exploited in the devices. Indeed, ZnO is a semiconductor with an intrinsic n-type behavior. The presence of free charges leads to a screening effect which reduces the charge accumulation and the consequent electric potential generation due to piezoelectricity.[30] When a conductive material is deposited on top of the microparticles, that is, GO, this phenomenon is enhanced and the material is not able to accumulate any electric potential at its electrodes. An insulating material like pHEMA, instead, can inhibit the charge transport, leading to a higher charge accumulation and a higher electric potential. When pHEMA is

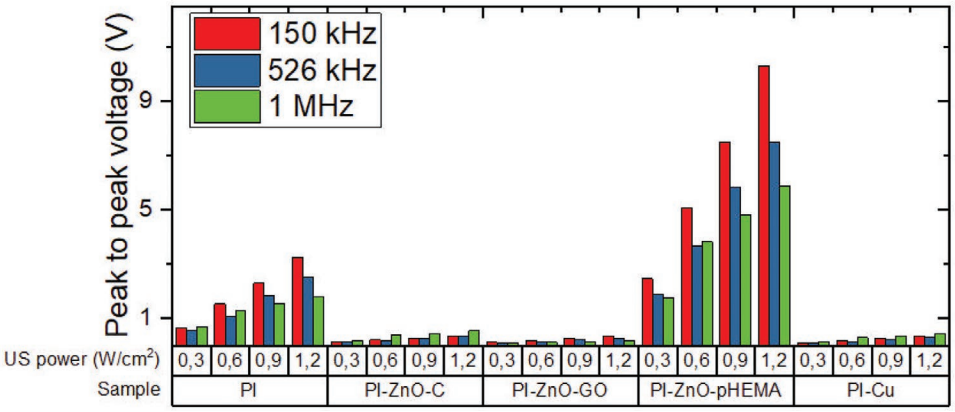

Figure 8. Maximum voltage generation between the bottom and the top of the different devices by mechanical deformation induced by various frequencies US stimulation.

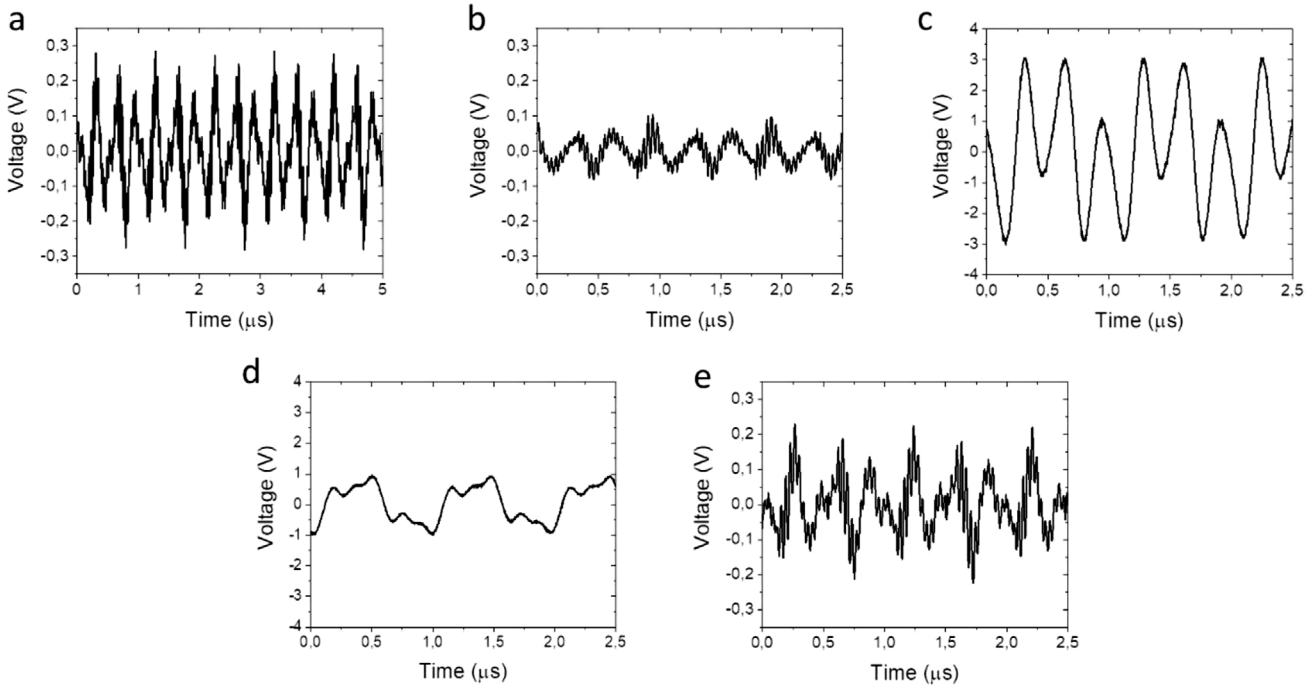

Figure 9. Representative voltage waveforms obtained during US stimulation (1 MHz US frequency and 1.2 W cm^{-2}). a) PI-ZnO-C, b) PI-ZnO-GO, c) PI-ZnO-pHEMA, d) PI, e) PI-Cu.

coupled to ZnO, the triboelectric effect that is observed also for the bare PI sample, is summed up to the piezoelectric potential generated by ZnO under US stimulation, resulting as the best device in terms of electro-mechanical response among the analyzed ones.

Some considerations on the devices can be also given considering their behavior at different frequencies. Indeed, for PI and PI-ZnO-pHEMA, the lower is the frequency, the higher is the amplitude of the signal. The reason for this may be linked to their insulating behavior and their consequent similarity with a two-parallel plate capacitor, which is characterized by a lower impedance as the frequency is increased. This behavior is not observed in the PI-Cu and PI-ZnO-C and PI-ZnO-GO samples. As a matter of fact, the 1 MHz stimulation results in a higher amplitude of the signal read by the oscilloscope. Determine the reason for this behavior is far to be trivial and must be linked to both triboelectric and piezoelectric phenomena which have to be decoupled for a more detailed analysis. However, the main goal of these devices is their ability to induce an electrical stimulation on a biological entity by means of a remote mechanical stimulation.

In **Figure 9**, a representative image for all the analyzed devices is reported for a 1 MHz US stimulation. The measurement of the period of the resulting waveforms allows to establish that the frequency of the electrical signal is the same as the US stimulation, suggesting the dependency of one phenomenon on the other. Moreover, the resulting waveform resembles what is typically found in the literature for the open circuit voltages of electromechanically-active films, in which a charging phase is immediately followed by a discharge phase when a mechanical stimulation is applied onto them.[53] It is however worth noticing that the obtained waveform present symmetricity on the voltage axis. This is given by the sinusoidal symmetricity of the US stimulation, confirming again the relationship between the electrical output and the mechanical stimulus.

Another interesting property of ZnO microparticles is their capability to generate ROS upon US stimulation.[54] The ability to modulate this phenomenon may represent a valuable tool because, on one side, an enhanced ROS generation can be exploited either for improved vascularization in healthy tissue during healing or for cancer therapy, while, on the other side, an excessive generation may be harmful for healthy cells.

Therefore, the ROS generation of PI, PI-ZnO, PI-ZnO-pHEMA, PI-ZnO-GO under US stimulation at 1 MHz for 1 min has been evaluated. In particular, the concentration of a specific radical species, that is, hydroxyl radical, has been evaluated through electron paramagnetic resonance (EPR) spectroscopy with the help of a chemical trap (DMPO) aimed at the radical life-time increase (see Section 4.4). The spectrum retrieved by the EPR measurements (**Figure 10a**) can be associated to the DMPO-OH complex,[55] assuring the generation of this species during US stimulation.

A quantitative analysis can be also performed evaluating the areas below the retrieved spectra. The results are reported in Figure 10b. In particular, the PI sample is used as control for the device. As it is possible to see, the PI-ZnO sample produces ROS already at 0.6 Wcm^{-2} of US power, while PI-ZnO-pHEMA and PI-ZnO-GO presented a detectable generation only from 0.9 Wcm^{-2} and with a magnitude lower than the sample of bare PI used as control. Indeed, simple water has been already demonstrated to generate ROS under US stimulation without the addition of any further component because of the cavitation

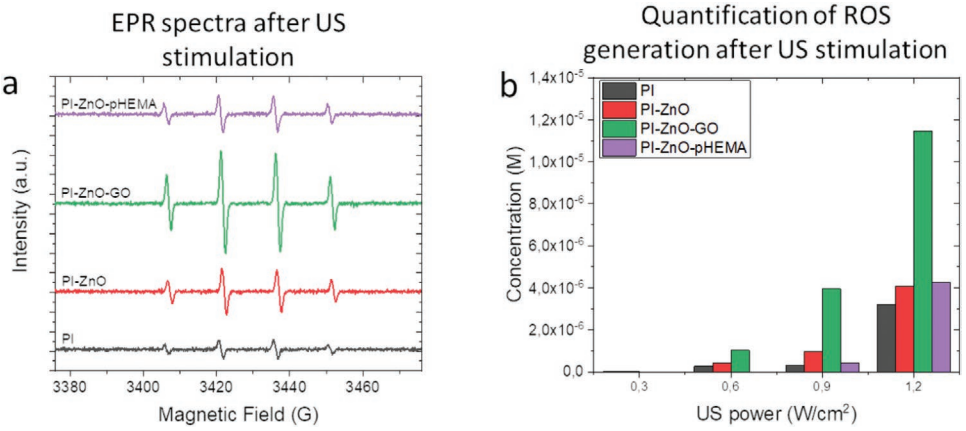

Figure 10. a) Representative images of the spin-adduct of the DMPO-OH complex retrieved by US stimulation of the devices for 1 min at 1 MHz and 1.2 W cm^{-2}, b) spin concentration evaluated by EPR analyses of the different samples after US stimulation for 1 min at 1 MHz.

induced by the periodical mechanical stimulation on gas microbubbles trapped in the liquid.[56] ZnO nanostructured materials may reduce the threshold for inertial cavitation because of the gas microbubbles adsorbed on their surface,[57] explaining the enhanced ROS generation found for the PI-ZnO sample, where high surface area microparticles are employed.

PI-ZnO-pHEMA sample presents ROS concentrations lower than the PI-ZnO film up to 0.9 Wcm^{-2}, while a comparable value between the two systems is found at 1.2 Wcm^{-2}. Therefore, the pHEMA layer seems to inhibit the generation of ROS under US stimulation, reducing the amount to values comparable with the control up to 0.9 Wcm^{-2}. The reason may lay in the uniform coverage of the ZnO microparticles that prevents the interaction of the semiconductor particles with water and the consequent cavitation threshold reduction.

The ROS production obtained with the PI-ZnO-GO sample is greatly enhanced with respect to the PI-ZnO system. The reason for this behavior is difficult to extrapolate, since GO has shown to increase the amount of ROS generated of 1 mL solution also without ZnO (Figure S3, Supporting Information). However, the combination of the two systems generates a synergistic effect which raises a lot the ROS concentration in the water after just 1 min of US stimulation. One of the reasons may be the different amount of gas trapped in the system. Indeed, the distribution of the GO layers on the ZnO microparticles may have induced a higher amount of gas trapped inside the system that may contribute to the inertial cavitation induced by the periodical mechanical stimulation.

In summary, PI-ZnO samples are able to produce an electrical potential and induce the generation of hydroxyl radicals when under US stimulation. However, pHEMA and GO layers are able to tune this ability. In one case, pHEMA was proved to increase the maximum open circuit voltage of the system, while the ROS generation was slightly reduced, with potential uses whenever an electrical stimulation is required and the system has to be highly biocompatible. On the other side, GO coating revealed to have an enhanced ROS generation under US irradiation suggesting its use in applications like sonodynamic therapy.

2.5. Biological Characterization

As a proof of concept, the optimized DR-ZnO films (PI-ZnO, PI-ZnO-GO, and PI-ZnO-pHEMA) were tested on an osteoblast-like cell line (SaOS-2) often used as model for bone tissue engineering[58] so as to have a preliminary evaluation of the biocompatibility features and potential applications of the developed devices. In particular, a Live/Dead assay coupled with fluorescence microscopy was exploited to assess the cell response to the developed substrates. All devices were also prepared without ZnO layer, as control substrates enabling identification of the specific role of the ZnO layer in cell behavior.

Figure 11a reports representative images of SaOS-2 cells stained with the Live/Dead assay reagents. The analysis held after 24 and 72 h of incubation shows that cells are able to adhere on the PI control sample, while the absence of any red signal (which indicates dead cells) suggests the high level of biocompatibility of the substrate. The GO coating does not influence the cell viability as well (Figure S4, Supporting Information). Indeed, all the cells are stained in green (indicating alive cells) and the cells shape is similar to the ones of the control sample. At 72 h from seeding, the cell number appears to be increased indicating regular cell proliferation on both control samples. A different situation is found on pHEMA. In fact, cells are not able to adhere on the PI-pHEMA control sample and retain the round shape due to trypsinization (Figure S4, Supporting Information). This is due to the cell-repulsive activity of the polymer which prevents cell adhesion and induces cell clustering[59–61] as it can be clearly seen also in Figure 11.

The incorporation of a DR-ZnO film in the device changes cell response. Indeed, cells are not able to adhere on the PI-ZnO sample and the presence of cell clusters can be clearly spotted in the fluorescence image representative of the device after 24 h from cell seeding. Moreover, there are some cells which show a red signal, indicating their death. The toxicity of nanostructured ZnO has been widely analyzed in literature and represents the main factor influencing ROS generation, the release of zinc cations in biological media, and the cell membrane damage.[28,62,63] Since no treatment was applied on cultured cells and the PI-ZnO sample showed no generation of

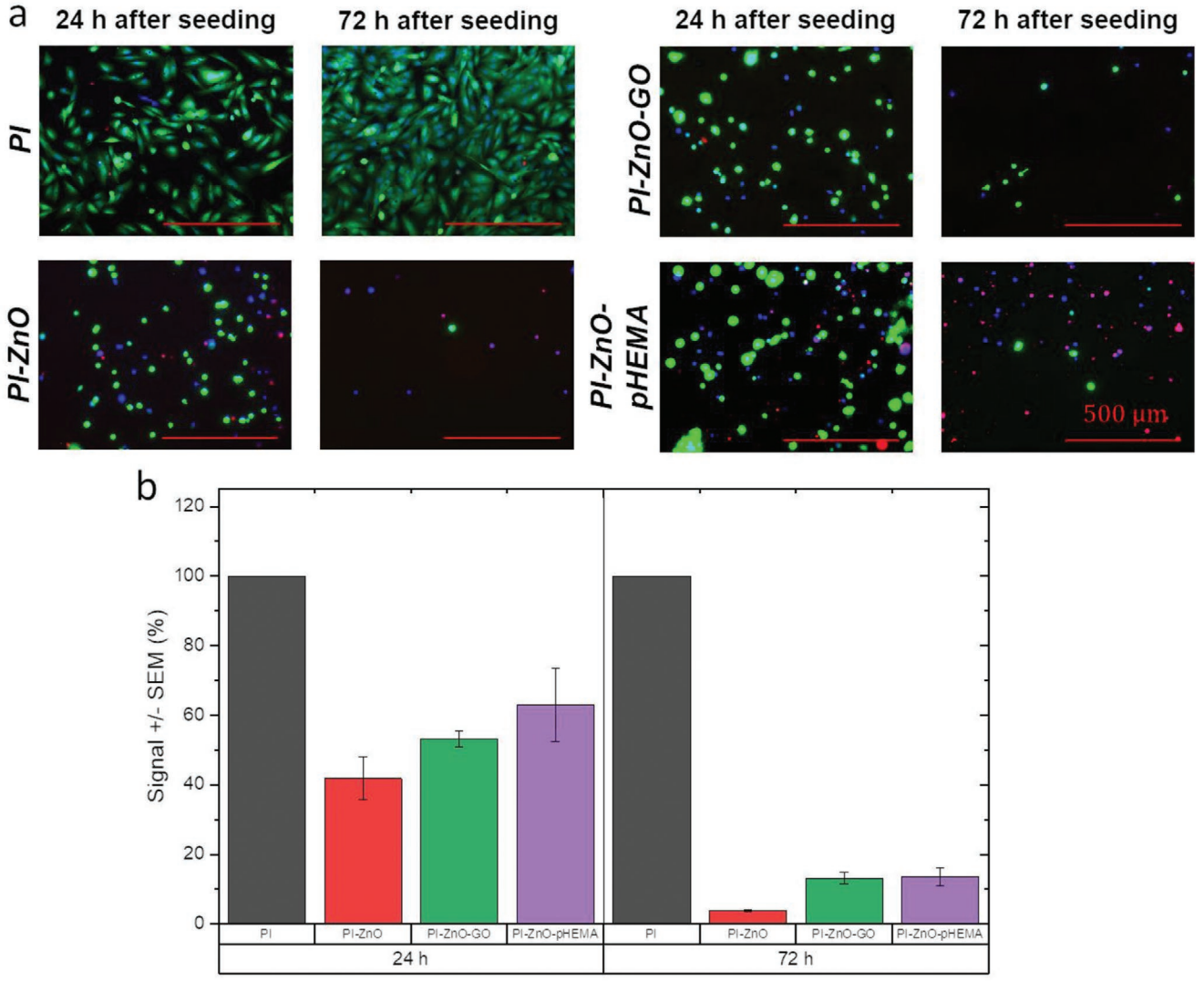

Figure 11. a) Representative image of fluorescence microscopy of SaOS-2 cell cultures after L/D staining. Live cells (green), dead cells (red), and cell nuclei (blue) are evidenced in images. b) Intensity quantification from fluorescence microscopy of SaOS-2 cell cultures after L/D staining on live cells at 24 and 72 h of incubation.

ROS at low US stimulation, it is fair to assume that cell death does not depend on ROS generation in this case. Therefore, the toxicity of this sample may be attributed to the dissolution of ZnO into zinc cations or to substrate roughness.

The addition of GO and pHEMA coatings slightly improved the biocompatibility of the system. In fact, PI-ZnO-GO and PI-ZnO-pHEMA showed a higher fluorescence signal coming from alive cells on the device with respect to the one found on the PI-ZnO sample (Figure 11b shows a quantitative estimation of the amount of green fluorescence signal obtained during the Live/Dead assay). In the case of the GO coating, this can be attributed to a slightly higher cell adhesion to the substrate which leads to a larger number of cells on the film.[35] Moreover, after 72 h from cell seeding, there are still few cells attached on the surface even if, again, lower in number with respect to 24 h of incubation. The pHEMA layer deposited on top of the device seems to increase even more the viable cells on the device. Probably this happens because the better conformal coating leads to a better screening of the typical cytotoxic phenomena of ZnO microparticles. However, the cell-repulsive properties of pHEMA prevent cell attachment, inhibiting cell proliferation at 72 h from seeding.

From this qualitative analysis, it is clear that DR-ZnO-based substrate presents potentialities in terms of tuning of biocompatibility and cell adhesion. In particular, the PI-ZnO-GO sample can be seen as a platform for drug delivery devices.[35] In contrast, the PI-ZnO-pHEMA can be considered an example of cell-repulsive device useful for instance to implants, catheters, that is, ureteral stents applications, as previously reported.[64]

In summary, the PI-ZnO-based substrates here described can easily be modified and exploited in view of the fabrication of multifunctional devices, that are able to kill cancer cells when required, while sustaining healthy tissue regrowth.[65] From the tumor-killing perspective, the ZnO substrate can be exploited either to produce ROS under US stimulation thanks to the synergistic effect with the GO coating or to inhibit tumor regrowth

on the substrate thanks to the poor pHEMA adhesion properties. On the other side, the antimicrobial properties of ZnO can prevent the rising of infections in long term treatments.

3. Conclusion

In this work we propose a novel smart and stimuli-responsive film based on desert-rose-like zinc oxide particles (DR-ZnO) and we demonstrate how the film surface properties can be tuned in terms of both functionalities and biocompatibility, depending on a required specific application.

ZnO microparticles presenting a desert-rose morphology were thus synthesized by means of a simple sol–gel hydrothermal method. The structural and morphological characterizations allowed to recognize their single phase wurtzitic crystallographic structure and their high surface area due to desert rose-like morphology.

To deposit the film onto flexible PI substrate, a paste of ZnO particles was prepared including ethanol, water, and acetic acid as dispersants. Acetic acid was effectively used to increase the dispersibility of the microparticles, however, its use causes the slight dissolution of ZnO and the precipitation of a new phase of zinc acetate (LHZA). An opportune thermal treatment was thus applied to restore the single ZnO wurtzitic phase and the original desert-rose morphology, as well as a fine optimization in terms of film uniformity and wetting behavior was also adopted.

Graphene oxide and pHEMA were proposed as additional functional layers to prove the possibility to adapt the proposed device to various biomedical applications.

Indeed, the addition of graphene oxide layer imparts to the overall device a larger generation of hydroxyl radicals and a moderate electric potential under US stimulation. A good biocompatibility was also found with osteoblast-like cells. These results suggest that further optimization of this device could lead to a completely biocompatible system for prolonged time frames, able to exploit the great potentialities of ZnO in bone tissue treatments.

The coating with pHEMA was shown to reduce the generation of ROS under US stimulation. However, a great enhancement of the electric potential generated under the same treatment was found indeed. Poor cell adhesion but enhanced biocompatibility were also obtained on pHEMA coated ZnO layers, indicating a potential application in medical devices where cell adhesion has to be avoided.

In conclusion, our newly developed films based on DR-ZnO can be efficiently activated remotely by US and their biocompatible properties and functionalities further improved by the addition of organic surface layers based on graphene oxide or polymers.

4. Experimental Section

Powder Synthesis: ZnO microparticles having a desert roses-like morphology were synthesized by means of a simple sol-gel hydrothermal technique already exploited in various works.[54,64] More in detail, 14.6 g of zinc nitrate hexahydrate ($Zn(NO_3)_2{\cdot}6H_2O$, Sigma-Aldrich) were dissolved in 100 mL of bi-distilled water. At the same time, 5.58 g of potassium hydroxide (KOH, Sigma-Aldrich) were dissolved in other 100 mL of bi-distilled water as well, in a Teflon container. To obtain the microparticles, the zinc nitrate solution was dropped into the potassium hydroxide one with a drop rate of about 1 drop sec^{-1} and the solution was kept in vigorous stirring up to the formation of a white gel. After that, the Teflon container was placed in an oven and treated at 70 °C for 4 h. Finally, the microparticles were separated by the solution through a 2 µm particle retention filter, washed with bi-distilled water, and dried overnight at 60 °C.

Film Fabrication: To obtain the film, the DR-ZnO microparticles were deposited onto a PI substrate (Kapton, DuPont). This was performed by dispersing the ZnO powder in an ethanol–water solution to which a small amount of acetic acid (glacial, PhEur) was added to increase the dispersibility. The final result was a paste that can be used to coat the PI substrate and whose deposition procedure is summarized in **Figure 12**.

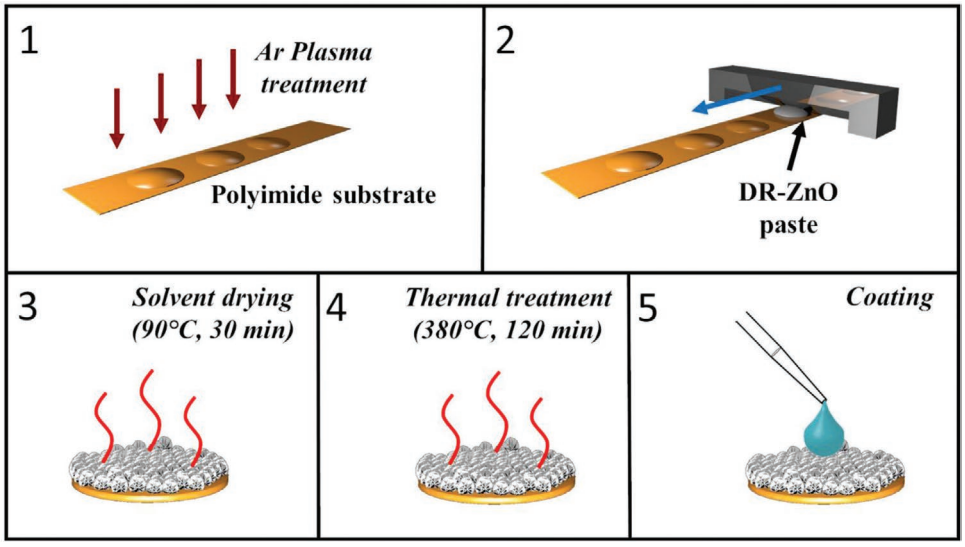

Figure 12. Schematics of the DR-ZnO films fabrication. 1) The PI substrate is treated with Argon plasma to increase its hydrophilicity; 2) then the DR-ZnO paste is deposited onto the substrate and 3) the film is left drying at 90 °C for 30 min. 4) A final thermal treatment is performed at 380 °C for 120 min. 5) An organic coating is finally deposited by drop-casting.

Table 2. Paste compositions analyzed during the optimization of the ZnO film fabrication.

Sample name	Acetic acid [% vol.]	Water [% vol.]	Ethanol [% vol]	Volume [mL]	ZnO powder [g]
PI-ZnO-A	0.8	32.7	66.5	2.325	1
PI-ZnO-B	0.8	32.7	66.5	2.325	0.5
PI-ZnO-C	0.4	32.8	66.8	2.315	0.5

The ZnO paste has been optimized in terms of solvent composition. The amount of solvent exploited, related to the amount of powder dispersed, is reported in **Table 2**. To prepare the paste required for the deposition, the DR-ZnO microparticles were weighed and placed in a glass vial. Then, acetic acid, bi-distilled water, and ethanol (99%, Sigma-Aldrich) were added to the powder in this order.

The compound was vigorously stirred for 10 min and placed for 30 min in a US bath (Labsonic LBS 2-10, Falc Instruments) at 40 kHz. Finally, the paste was kept in agitation with the magnetic stirrer before its use for at least 5 min.

For what concerns the PI substrate preparation, 4 circles having 1 cm of diameter were only partially cut on 1.5 cm × 6.5 cm PI strips so as to keep them in their place while performing the Argon plasma treatment exploited to increase the hydrophilicity of the material. The latter was performed with a QUORUM Q150T-S sputter coater at 30 mA for different times during the optimization (1, 2, 5 min). The optimized recipe sees the 2 min treatment as the best one. Afterward, the plasma-treated samples were flattened on a glass slide and covered with a PVC adhesive tape (75 µm thickness, Nitto) that acted as template for the round samples.

On the top of the strip, 50 µL of ZnO paste was deposited and spun with a steel template up to the coverage of all the circles. The coated strip was placed on a hot plate set at 90 °C for 30 min in order to evaporate all the solvents. The circles were removed from the strip and placed again on a hot plate at 380 °C for 2 h to obtain the final PI-ZnO sample.

The samples were then coated with either a graphene oxide (GO, CheapTubes, 300–800 nm lateral dimensions) or poly(2-hydroxyethyl methacrylate) (pHEMA, obtained from HEMA monomers from Sigma-Aldrich, according to the procedure described in another work[64]) layer.

Commercial GO powders were dissolved into bi-distilled water at 0.5 mg mL^{-1} by the help of a 10-min sonication and deposited by drop-casting. In particular, 20 µL of GO solution was deposited onto the PI-ZnO substrate. When the solvent evaporated, the process was repeated for other two times.

pHEMA-coated samples (PI-ZnO-pHEMA) were again obtained by drop-casting starting from a 10% w/v methanol solution in which the dried polymer was dissolved. In particular, 12 µL of pHEMA solution was drop-casted onto the PI-ZnO sample and left drying overnight to allow solvent evaporation.

Physico-Chemical Characterization: Both powders and films were characterized in terms of physico-chemical properties. XRD measurements were performed by a Panalytical X'Pert PRO diffractometer in Bragg-Brentano configuration, equipped with a CuKα monochromatic radiation (λ = 1.54 Å) as X-ray source. Morphology of all the samples was characterized by means of FESEM (Merlin, Zeiss). In the case of PI-ZnO-pHEMA, a thin platinum coating was deposited by means of a QUORUM Q150T-S sputter coater (30 mA, 10 s).

Attenuated total reflectance infrared spectroscopy (ATR-IR) was exploited to assess the chemistry of the surface of the samples and was performed with a NICOLET 5700 FTIR spectrometer (ThermoFisher). Each spectrum was acquired as the mean of 64 scans at a resolution of 2 cm^{-1} and background subtracted.

Contact angle measurements were performed with an OCAH 200 (DataPhysics Instruments Gmbh) OCA measuring system.

Film Functional Characterization: The devices were characterized in terms of electromechanical response and ROS generation upon US stimulation.

The evaluation of the electromechanical response of the developed devices required a change in the device design in order to collect the electrical signal due to US stimulation. A scheme of the new design is reported in **Figure 13**. To evaluate the electric potential that the US stimulation induces in the analyzed samples, it was required to have two electrodes: one on the top of the structure and one on the bottom. For what concerns the bottom electrode, commercial Cu-coated PI was used as substrate material. The optimized DR-ZnO microparticles paste was directly deposited onto the PI-Cu film by the help of the PVC tape template and without Argon plasma pre-treatment. The same thermal treatments described in Section 4.2 were then performed as well as the GO and pHEMA depositions.

To fabricate the top-electrode, four 2 mm-diameter platinum circles have been sputtered on the films (≈50 nm). Then, the active device was connected to an oscilloscope (Tektronix TDS2012B), setting the reference to the bottom electrode. The top electrode was put in direct contact with an opportunely shaped PI-Cu strip connected to the oscilloscope.

The measurements were performed by placing the samples on a piezoelectric transducer (LipoZero G39, Globus). To increase the acoustic coupling between the transducer and the sample, a water-based gel was spun between the US source and the active device.

The analyses were performed on the optimized devices (PI-ZnO, PI-ZnO-GO, and PI-ZnO-pHEMA) and on control samples (PI, and PI-Cu) with 3 US frequencies (150 kHz, 526 kHz, and 1 MHz) and 4 power values (0.3, 0.6, 0.9, and 1.2 Wcm^{-2}). Waveform analyses were performed with Matlab.

To study the generation of ROS during US stimulation, EPR spectroscopy (EPR) coupled with the spin trapping technique was exploited. In particular, the PI-ZnO, PI-ZnO-GO, and the PI-ZnO-pHEMA samples were placed in a 24-well plate (TC-treated, Corning) and subjected to 1 MHz US stimulation (0.3, 0.6, 0.9, and 1.2 Wcm^{-2}) for 1 min in a 1 mL aqueous solution of 5,5-Dimethyl-1-pyrroline N-oxide (DMPO, Sigma-Aldrich) at the concentration of 2.5 mM. As control, the same experiment was repeated by using a bare PI sample, so as to oppose the same impedance of the other analyzed sample to US propagation.

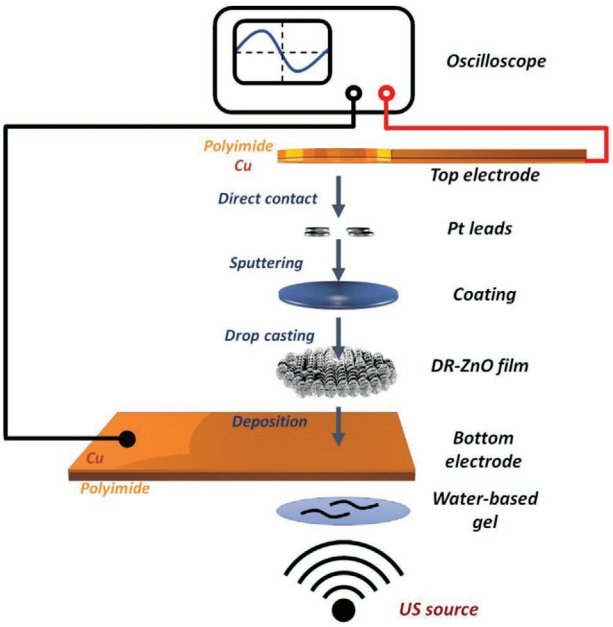

Figure 13. Schematics of the DR-ZnO films electromechanical characterization setup.

By means of a quartz capillary (volume 50 µL), a tiny amount of the solution was withdrawn by the well and inserted in the cavity of an EMX-Nano (Bruker) EPR spectrometer. The quantitative analysis was performed with Xenon-nano software.

Cell Culture: Osteoblast-like SaOS-2 cells (ATCC, HTB-85) were cultured in Dulbecco's Modified Eagle Medium (DMEM, Sigma-Aldrich) supplemented with 10% of Fetal Bovine Serum (FBS), 2 mM L-glutamine, and 100 U mL^{-1} penicillin-100 µg mL^{-1} streptomycin solution. Cells were grown in incubator at a temperature of 37 °C and with 5% CO_2 atmosphere. Cell culture medium was changed every two days and cells were split on different Petri dishes when they reached ≈70% confluence.

Live/Dead Assay: To assess the biocompatibility of the fabricated substrates (PI, PI-ZnO, PI-ZnO-GO, and PI-ZnO-pHEMA), a Live/Dead (L/D) assay coupled with fluorescence microscopy was performed. First of all, all the samples were placed at the bottom of a 24-well plate and pre-incubated with 500 µL of cell culture medium for 1 h at 37 °C in order to promote the device coating with serum proteins. Before cell seeding, cell medium was replaced. Cells were seeded by adding 200 µL of cell suspension in order to have a surface density of 10^4 cells cm^{-2}. L/D assays were performed after 24 and 72 h of incubation at 37 °C. To stain cells, at the end of each incubation time, the cell culture medium was removed. Then, 200 µL of DMEM without phenol red and supplemented with 10% of FBS, 2 µL mL^{-1} of calcein-AM, 2 µL mL^{-1} of ethidium homodimer (Life Technologies) and 8 µL mL^{-1} of Hoechst (Sigma) were added to each well. The three dyes respectively stain healthy, dead cells, and cell nuclei, respectively.

After 5 min of incubation at 37 °C and 5% of CO_2, the staining solution was removed and 200 µL of 10% FBS-DMEM without phenol red was added. Fluorescence microscopy was performed with a Nikon Eclipse Ti microscope equipped with a super high-pressure mercury lamp.

A quantitative estimation of the amount of fluorescence got during fluorescence measurements was performed through Matlab on three different images for each sample. More in detail, each image was divided into its three color components (green, red, and blue), so as to separate the intensity of each channel corresponding to the live (green) and dead (red) cells, as well as the presence of nuclei (blue), for each pixel. The green channel was considered to compare the amount of signal retrieved by alive cells in each of the system analyzed. The value contained in each pixel of the image was summed after the subtraction of the background and normalized with respect to the value obtained for the PI control sample.

Supporting Information

Supporting Information is available from the Wiley Online Library or from the author.

Acknowledgements

Part of this work has received funding from the European Research Council (ERC) under the European Union's Horizon 2020 research and innovation programme (grant agreement no. 678151—Project Acronym "TROJANANOHORSE"—ERC starting Grant).

Open Access Funding provided by Politecnico di Torino within the CRUI-CARE Agreement.

Conflict of Interest

The authors declare no conflict of interest.

Data Availability Statement

Research data are not shared.

Keywords

graphene oxide, pHEMA, reactive oxygen species (ROS), ultrasound, ZnO

Received: June 18, 2021
Revised: July 30, 2021
Published online:

[1] P. Tartaj, M. a del P Morales, S. Veintemillas-Verdaguer, T. G. lez-Carre o, C. J. Serna, *J. Phys. D: Appl. Phys.* **2003**, *36*, R182.
[2] M. A. C. Stuart, W. T. S. Huck, J. Genzer, M. Müller, C. Ober, M. Stamm, G. B. Sukhorukov, I. Szleifer, V. V. Tsukruk, M. Urban, F. Winnik, S. Zauscher, I. Luzinov, S. Minko, *Nat. Mater.* **2010**, *9*, 101.
[3] Z. L. Wang, *Nano Res.* **2008**, *1*, 1.
[4] X. Wang, J. Liu, J. Song, Z. L. Wang, *Nano Lett.* **2007**, *7*, 2475.
[5] G. Ciofani, S. Danti, D. D'Alessandro, L. Ricotti, S. Moscato, G. Bertoni, A. Falqui, S. Berrettini, M. Petrini, V. Mattoli, A. Menciassi, *ACS Nano* **2010**, *4*, 6267.
[6] M. Hoop, X.-Z. Chen, A. Ferrari, F. Mushtaq, G. Ghazaryan, T. Tervoort, D. Poulikakos, B. Nelson, S. Pané, *Sci. Rep.* **2017**, *7*, 4028.
[7] J.-K. Yoon, M. Misra, S. J. Yu, H. Y. Kim, S. H. Bhang, S. Y. Song, J.-R. Lee, S. Ryu, Y. W. Choo, G.-J. Jeong, S. P. Kwon, S. G. Im, T. I. Lee, B.-S. Kim, *Adv. Funct. Mater.* **2017**, *27*, 1703853.
[8] C. Ribeiro, V. Sencadas, D. M. Correia, S. Lanceros-Méndez, *Colloids Surf., B* **2015**, *136*, 46.
[9] A. Marino, S. Arai, Y. Hou, E. Sinibaldi, M. Pellegrino, Y.-T. Chang, B. Mazzolai, V. Mattoli, M. Suzuki, G. Ciofani, *ACS Nano* **2015**, *9*, 7678.
[10] G. G. Genchi, L. Ceseracciu, A. Marino, M. Labardi, S. Marras, F. Pignatelli, L. Bruschini, V. Mattoli, G. Ciofani, *Adv. Healthcare Mater.* **2016**, *5*, 1808.
[11] A. Marino, E. Almici, S. Migliorin, C. Tapeinos, M. Battaglini, V. Cappello, M. Marchetti, G. de Vito, R. Cicchi, F. S. Pavone, G. Ciofani, *J. Colloid Interface Sci.* **2019**, *538*, 449.
[12] B. Yang, Y. Chen, J. Shi, *Chem. Rev.* **2019**, *119*, 4881.
[13] A. Ancona, B. Dumontel, N. Garino, B. Demarco, D. Chatzitheodoridou, W. Fazzini, H. Engelke, V. Cauda, *Nanomaterials* **2018**, *8*, 143.
[14] D. E. J. G. J. Dolmans, D. Fukumura, R. K. Jain, *Nat. Rev. Cancer* **2003**, *3*, 380.
[15] G. Canavese, A. Ancona, L. Racca, M. Canta, B. Dumontel, F. Barbaresco, T. Limongi, V. Cauda, *Chem. Eng. J.* **2018**, *340*, 155.
[16] M. Laurenti, V. Cauda, *Nanomaterials* **2017**, *7*, 374.
[17] B. Dumontel, F. Susa, T. Limongi, M. Canta, L. Racca, A. Chiodoni, N. Garino, G. Chiabotto, M. L. Centomo, Y. Pignochino, V. Cauda, *Nanomedicine* **2019**, *14*, 2815.
[18] M. J. Akhtar, M. Ahamed, S. Kumar, M. M. Khan, J. Ahmad, S. A. Alrokayan, *Int. J. Nanomed.* **2012**, *7*, 845.
[19] D. Ilager, N. P. Shetti, R. S. Malladi, N. S. Shetty, K. R. Reddy, T. M. Aminabhavi, *J. Mol. Liq.* **2021**, *322*, 114552.
[20] M. M. Shanbhag, N. P. Shetti, R. M. Kulkarni, P. Chandra, *Microchem. J.* **2020**, *159*, 105409.
[21] D. R. Kulkarni, S. J. Malode, K. Keerthi Prabhu, N. H. Ayachit, R. M. Kulkarni, N. P. Shetti, *Mater. Chem. Phys.* **2020**, *246*, 122791.
[22] N. P. Shetti, S. D. Bukkitgar, K. R. Reddy, Ch. V. Reddy, T. M. Aminabhavi, *Biosens. Bioelectron.* **2019**, *141*, 111417.
[23] N. P. Shetti, S. J. Malode, D. Ilager, K. Raghava Reddy, S. S. Shukla, T. M. Aminabhavi, *Electroanalysis* **2019**, *31*, 1040.
[24] M. Laurenti, V. Cauda, *Materials* **2018**, *11*, 314.
[25] X. Xu, D. Chen, Z. Yi, M. Jiang, L. Wang, Z. Zhou, X. Fan, Y. Wang, D. Hui, *Langmuir* **2013**, *29*, 5573.

[26] A. Azam, A. S. Ahmed, M. Oves, M. S. Khan, S. S. Habib, A. Memic, *Int. J. Nanomed.*, 7.
[27] N. Daneshvar, D. Salari, A. R. Khataee, *J. Photochem. Photobiol., A* **2004**, *162*, 317.
[28] M. Carofiglio, S. Barui, V. Cauda, M. Laurenti, *Appl. Sci.* **2020**, *10*, 5194.
[29] G. Ciofani, G. G. Genchi, V. Mattoli, *Mater. Sci. Eng., C* **2012**, *32*, 341.
[30] M. Laurenti, G. Canavese, A. Sacco, M. Fontana, K. Bejtka, M. Castellino, C. F. Pirri, V. Cauda, *Adv. Mater.* **2015**, *27*, 4218.
[31] H.-M. Xiong, *Adv. Mater.* **2013**, *25*, 5329.
[32] I. Brigger, C. Dubernet, P. Couvreur, *Adv. Drug Delivery Rev.* **2002**, *54*, 631.
[33] L. Racca, T. Limongi, V. Vighetto, B. Dumontel, A. Ancona, M. Canta, G. Canavese, N. Garino, V. Cauda, *Front. Bioeng. Biotechnol.* **2020**, *8*.
[34] C. Brazzale, R. Canaparo, L. Racca, F. Foglietta, G. Durando, R. Fantozzi, P. Caliceti, S. Salmaso, L. Serpe, *Nanomedicine* **2016**, *11*, 3053.
[35] M. Laurenti, A. Lamberti, G. G. Genchi, I. Roppolo, G. Canavese, C. Vitale-Brovarone, G. Ciofani, V. Cauda, *ACS Appl. Mater. Interfaces* **2019**, *11*, 449.
[36] V. Cauda, D. Pugliese, N. Garino, A. Sacco, S. Bianco, F. Bella, A. Lamberti, C. Gerbaldi, *Energy* **2014**, *65*, 639.
[37] A. L. Patterson, *Phys. Rev.* **1939**, *56*, 978.
[38] M. Hasegawa, K. Horie, *Prog. Polym. Sci.* **2001**, *26*, 259.
[39] K.-Y. Law, *J. Phys. Chem. Lett.* **2014**, *5*, 686.
[40] V. Gandhi, R. Ganesan, H. H. Abdulrahman Syedahamed, M. Thaiyan, *J. Phys. Chem. C* **2014**, *118*, 9715.
[41] M. Ristić, S. Musić, M. Ivanda, S. Popović, *J. Alloys Compd.* **2005**, *397*, L1.
[42] G. Socrates, *Infrared and Raman Characteristic Group Frequencies: Tables and Charts*, Wiley, Chichester, **2010**.
[43] E. Hosono, S. Fujihara, T. Kimura, H. Imai, *J. Sol-Gel Sci. Technol.* **2004**, *29*, 71.
[44] M. Saito, S. Fujihara, *Energy Environ. Sci.* **2008**, *1*, 280.
[45] Y. Arima, H. Iwata, *Biomaterials* **2007**, *28*, 3074.
[46] G. Wang, Y. Ma, Z. Wei, M. Qi, *Chem. Eng. J.* **2016**, *289*, 150.
[47] D. Chen, H. Feng, J. Li, *Chem. Rev.* **2012**, *112*, 6027.
[48] A. Konwar, S. Kalita, J. Kotoky, D. Chowdhury, *ACS Appl. Mater. Interfaces* **2016**, *8*, 20625.
[49] P. Tenke, C. R. Riedl, G. L. Jones, G. J. Williams, D. Stickler, E. Nagy, *Int. J. Antimicrob. Agents* **2004**, *23*, 67.
[50] P. Tenke, B. Köves, K. Nagy, S. J. Hultgren, W. Mendling, B. Wullt, M. Grabe, F. M. E. Wagenlehner, M. Cek, R. Pickard, H. Botto, K. G. Naber, T. E. Bjerklund Johansen, *World J. Urol.* **2012**, *30*, 51.
[51] M. Laurenti, M. Grochowicz, V. Cauda, *Coatings* **2018**, *8*, 376.
[52] X. Ma, H. Wang, S. Jin, Y. Wu, X.-J. Liang, *Int. J. Nanomed.* **2012**, *7*, 1313.
[53] P. Thakur, A. Kool, N. A. Hoque, B. Bagchi, F. Khatun, P. Biswas, D. Brahma, S. Roy, S. Banerjee, S. Das, *Nano Energy* **2018**, *44*, 456.
[54] C. Lops, A. Ancona, K. Di Cesare, B. Dumontel, N. Garino, G. Canavese, S. Hérnandez, V. Cauda, *Appl. Catal., B* **2019**, *243*, 629.
[55] G. R. Buettner, *Free Radicals Biol. Med.* **1987**, *3*, 259.
[56] V. Vighetto, A. Ancona, L. Racca, T. Limongi, A. Troia, G. Canavese, V. Cauda, *Front. Bioeng. Biotechnol.* **2019**, *7*, 374.
[57] A. Ancona, A. Troia, N. Garino, B. Dumontel, V. Cauda, G. Canavese, *Ultrason. Sonochem.* **2020**, *67*, 105132.
[58] M. Prideaux, A. R. Wijenayaka, D. D. Kumarasinghe, R. T. Ormsby, A. Evdokiou, D. M. Findlay, G. J. Atkins, *Calcif. Tissue Int.* **2014**, *95*, 183.
[59] S. Tugulu, P. Silacci, N. Stergiopulos, H.-A. Klok, *Biomaterials* **2007**, *28*, 2536.
[60] M. E. Katt, A. L. Placone, A. D. Wong, Z. S. Xu, P. C. Searson, *Front. Bioeng. Biotechnol.* **2016**, 4.
[61] J. Friedrich, C. Seidel, R. Ebner, L. A. Kunz-Schughart, *Nat. Protoc.* **2009**, *4*, 309.
[62] A. Sirelkhatim, S. Mahmud, A. Seeni, N. H. M. Kaus, L. C. Ann, S. K. M. Bakhori, H. Hasan, D. Mohamad, *Nano-Micro Lett.* **2015**, *7*, 219.
[63] T. Xia, M. Kovochich, M. Liong, L. Mädler, B. Gilbert, H. Shi, J. I. Yeh, J. I. Zink, A. E. Nel, *ACS Nano* **2008**, *2*, 2121.
[64] M. Laurenti, M. Grochowicz, E. Dragoni, M. Carofiglio, T. Limongi, V. Cauda, *Materials* **2020**, *13*, 3821.
[65] J. Liao, R. Han, Y. Wu, Z. Qian, *Bone Res.* **2021**, *9*, 18.